Article

Persistence of strain in filament-motor assemblies

Arvind Gopinath[1,2,‡,*], Raghunath Chelakkot[3,‡], and L Mahadevan[4,*]

[1]Department of Bioengineering, University of California Merced, Merced, CA, USA 95340.
[2]Health Sciences Research Institute, University of California Merced, Merced, CA, USA 95340.
[3]Department of Physics, Indian Institute of Technology Bombay, Mumbai, India.
[4]Department of Physics, Department of Organismic and Evolutionary Biology, and School of Engineering and Applied Sciences, Harvard University, Cambridge, MA, USA.
[*]Correspondence: agopinath@ucmerced.edu, raghu@phy.iitb.ac.in, lmahadev@harvard.edu, †Equal contribution

ABSTRACT The spatial extent to which elastic deformations of cross-linked filaments persist in noisy active environments and the associated decay length plays a fundamental role in many biological settings. Here, we study the mechanical response of an active ordered composite comprised of elastic filaments sheared by active motors. We compare results from Brownian multi-particle collision dynamics-based numerical simulations for actively driven deformations of noisy and moderately soft composites with theoretical predictions from a mean-field theory valid in the noiseless and weakly elastic limit. Surprisingly, several qualitative features predicted by the noise-less mean field model are seen even in strongly noisy simulations. We find, from both theory and simulations, that even when extensibility is negligible locally, it cannot be ignored when considering global deformation fields. This is because the length scale over which extensional deformations persist is controlled by the competition between passive elasticity of the filament and active effective shear stiffening due to attached motors and other crosslinks. Specifically, for fixed motor kinetics and properties, the decay length of extensional deformations is controlled by the ratio of the passive elastic modulus of the composite to an effective active, motor generated shear modulus. For steady strains, the length scale is surprisingly independent of motor activity except when motors are in a state of rigor. For oscillatory strains, the persistence length may be varied strongly by changing the frequency of forcing. When the effect of noise is dominant, the strain fields on the filament becomes uncorrelated. Our study demonstrates how correlated activity in natural ordered active matter possesses a finite range of influence with testable experimental implications.

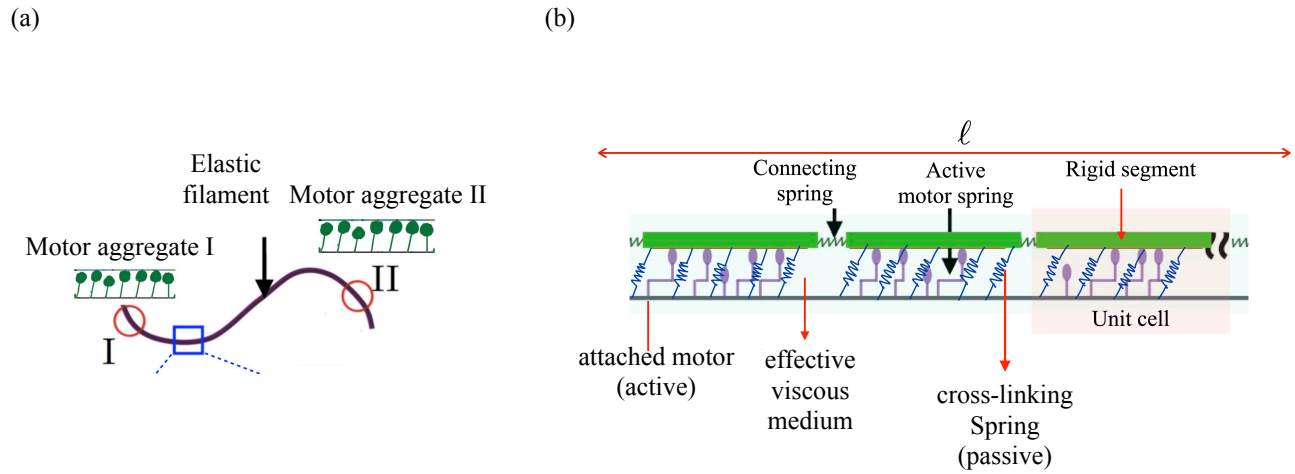

Figure 1: a) Schematic of a motor-filament composite filament with spatially separated motor aggregates at locations (I) and (II). The softer the intervening filament segment connecting (I) and (II), the higher the tendency of the motor groups to remain uncorrelated and unable to mechanically communicate. If motor aggregates (MT-1 and MT-2) are unable to communicate, coherent sliding and synchronization is prevented, and oscillations may remain localized or even decay eventually. (b) Schematic of the composite passive strip with extensional and shear deformations alone analyzed in the computational model. The continuous composite filament is treated in discrete fashion as a chain of small rigid segments attached to neighboring segments by linearly elastic springs. Each segment interacts with a locally homogenous population of motors. Motor populations interacting with spatially separated segments may have different properties.

1 INTRODUCTION

1.1 Motivation

The active strain generated by molecular motors interacting with biofilaments and networks is the principal mechanism of force generation and motion in cell biology (1–11). In these assemblies, soft bio-filaments are dynamically deformed and strained by localized, steady or time-dependent strains imposed by motors. The strength and intensity of these deformations depend on various factors including filament structure and elastic properties, on the density and elasticity of cross-linkers, on the mechanochemistry and kinetics of motor-filament attachments, and also on geometric constraints arising from boundary conditions. Additionally, athermal stochasticity due to variations in motor activity and finite motor number, and thermal noise from the temperature of the ambient medium may further impact deformation fields.

Filament-motor assemblies and networks are known to feature long-range mechanical interactions. It is relevant then to ask if mechanical force transmission mechanisms feature cut-off lengths and the manner in which emergent composite mechanical properties and activity. An example of this is recent experimental and theoretical work on motile non-adherent cells such as fibroblasts crawling on compliant soft surfaces, where mechanical inter-cell communication was noted to persists only to finite distances. More generally the decay lengths associated with loss of mechanically mediated communication may enable or limit function and physiology at intracellular and cellular scales. Here, we investigate a fundamental question that arises in this context - the length scale over which strain fields and deformations decay in active systems with noise.

To illustrate, in Fig. 1(a), we sketch two spatially separated and distinct motor aggregate patches (labeled I and II) that crosslink a pair of thin elastic filaments. Let us assume that the filament is inextensible but is still able to shear and bend. Mechanical activity by group I and shear stresses and deformation induced by this patch is transmitted by attached motors in group II over arbitrarily large inter-aggregate distances. Thus stiffness ensures coherence and coordination as motors in II can sense stress and deformations induced by motors in aggregate I. However, when the filament is extensible, ability of motors in group I to mechanically sense and sync with group II is limited. One may readily intuit that, for very soft filaments, localized strains and stresses induced at location I lead to propagating fields that decay rapidly along the filament, and are not therefore sensed by motors at II. Clearly, finite decay lengths for soft filaments imply that any transmission of mechanical information between spatially separated motor aggregates (here I and II) has a necessarily limited range, constrains coordinated activity and results in de-coherence.

Since many bio-filaments such as microtubules are intrinsically stiff in the absence of cross-linking filaments [*,*], filament

extensibility was usually neglected in studies on cross-linked filamentous networks. However, several recent models of passive filament bundles (7, 35–37) do account for finite stretching stiffness - the extensional elasticity - of the filaments. Experiments indicate that when such bundled filaments are bent, the characteristic length scale over which the mechanical information is transmitted is determined by a combination of the effective shear stiffness of the bundle, stretching, as well as the bending stiffnesses of the individual filaments. In particular, recent work by Ward *et. al* (37) on mutually sliding actin filaments suggests that the nontrivial dependance of sliding friction on the filaments' overlap length can be explained by a length-scale arising from the finite extensional rigidity of f-actin. These studies have identified the length scale over which mechanical strains in passive networks decay and have clarified the roles of shear and extensional modes of deformation in controlling this length. However, the emergence of analogous decay lengths in such active filament-motor assemblies remains to be understood.

1.2 Organization of results

As a concrete illustration of the implications resulting from the finite persistence lengths, we turn to the example of eukaryotic flagellum. This flexible, slender complex organelle is comprised of ordered assemblies of stiff microtubules, dynein ATPase motors and passive nexin proteins. It has been hypothesized that action of arrayed dynein motors on the microtubules coupled with geometric and elastic constraints convert sliding forces and motions into oscillations with well-defined frequencies and wavelengths (2, 13, 16–20, 33, 34). Models with varying degrees of complexity have been introduced to study these flagellar and similar filament-motor assemblies (3, 5–10, 20, 33, 34). Microtubules are typically assumed to be inextensible; this implies that localized extensional strains are felt across the whole filament irrespective of its length. A linear stability analysis for the onset of oscillations for such a flagella predicts that emergent wavelengths scale as the flagellar length without limit. This deduction is however at odds with experimental evidence that indicate that the beating wavelength of flagella are self-limiting even as the flagella themselves range from tens of microns to nearly a centimeter (2–4). We hypothesize that finite extensibility of the axoneme may impact overall bending, shear and extensional elasticity and result in limiting wavelengths. Additionally, kinetics of motor activity set by ATP hydrolysis rates can couple back to effective extensibility by introducing strong local shear stiffening that may induce weak but non-trivial stretching deformations.

Motivated by this example, we address the following questions which are also applicable to more general filament-motor assemblies and systems:

1. What is the effective coarse-grained elasticity of composite arrayed active filament-motor assembles?

2. What sets the length scale over which localized elastic strains persist in such systems?

3. How do overall elasticity and motor kinetics (such as attachment rates, detachment rates, duty ratio) vary with properties of the constituents and impact persistence length and emergent coordination? Motor groups interacting with an infinitely-stiff filament will eventually coordinate their dynamics resulting in coherent dynamics. Softness arising from different activity mediated elastic properties - extensional, shear, or even athermal noise - may disrupt this process and provide physical mechanisms by which this may be disrupted. To explore this hypothesis, we combine analytical and computational modes of interrogation of a minimal extension dominated system.

In section 2, we elucidate the coupling between bend, shear and extensional elastic components in a passive composite containing filaments and passive cross-linkers. We obtain the persistence of extensional and bending strains for a passive composite. In section 3 we use results from section 2 to derive mean-field equations for active filament-motor composites. Ignoring stochastic effects, we focus on the role of shear stiffening and strain softening in extensional systems and derive analytical expressions for the persistence lengths of extensional strain fields and obtain insights into when spatially separated and independently oscillating motor domains may synchronize. The theoretical analyses from sections 2 and 3 deal with noise-less systems. However, the onset of steady or oscillatory extension necessarily involves small numbers of motors when the deformation field develops from initially noisy states. We explore this limit in section 4, where we use a discrete stochastic numerical scheme for a model system depicted in Figure 1(b). The simulation incorporates athermal motor noise arising due to discrete nature of motor kinetics, and system size effects originating due to the finite number (density) of motors. Surprisingly, the predictions of the mean-field theory agree qualitatively with the results from stochastic discrete filament-motor model, even for moderately strong noise. For strong athermal motor noise, we predict rich dynamical features, including the modification of the motor duty-ratio, and localized regions of coherent oscillations.

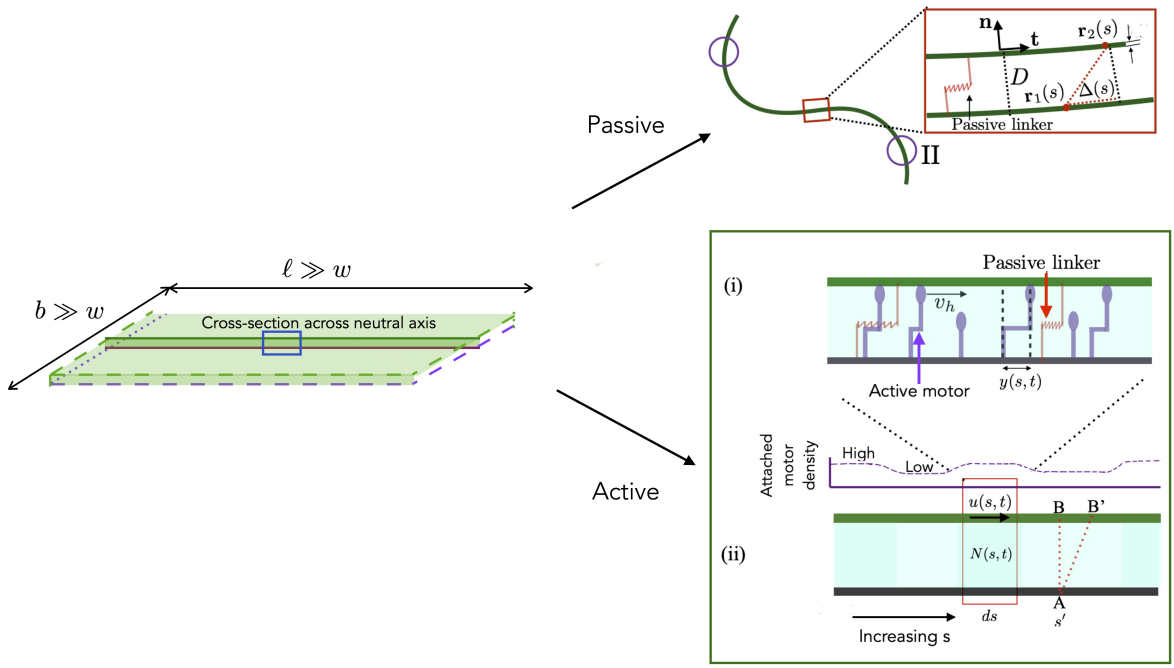

Figure 2: Geometry of the systems analyzed in §2 & §3. (Left tile) Schematic of the composite motor-filament. We consider two strips each of length ℓ, breadth b, and thickness w separated by a distance D. Length-scales $w \ll \ell$ and $w \ll b$; additionally the transverse direction may be treated as a neutral direction. A small portion of this marked in blue is magnified. Sketches of these are shown on the right for passive (right, top tile) and active (right, bottom tile) cases. (Upper, right tile) Passive composite system analyzed in §2. Motors are not present in this system. Deformational modes within the composite comprise geometrically coupled bending, stretching and shear modes. Both lower and upper sheets provide extensional and bending resistances. The passive cross-linkers maintaining the distance D provide the shear resistance. The thickness of the strip w is much smaller than the length ℓ and width b. (Upper, left tile) Cross-section of *active* motor-filament composite strip. We simplify the system further by now specifying that the bottom strip (purple dashed lines) is rigid and fixed. The upper strip (green dashed line) can stretch and slide but cannot bend. Further magnifying the composite filament illuminates the discrete elements comprising the continuous filament. Shown are the passive links (red) and active motors (purple) spanning the distance D. Motors attach with a pre-extension d_m and then move along the upper filament with speed v_h relative to their base. The mechanical stressed state of attached motors is quantified by their internal extension y. Coarse-graining motor activity provides the local density of attached motors $N(s,t)$ and the local mean motor extension $Y(s,t)$. Shown is a typical deformation (combination of slide/shear and extension) that moves material point B to B'.

2 MEAN-FIELD MODEL FOR PASSIVE ASSEMBLIES

2.1 Geometry and definitions

We start our analysis by studying a passive-filament systems - a composite assembly without motors. Consider Figure 2 (left tile) that illustrates the composite comprised of two cross-linked elastic strips (purple, and green). The strips have rest length ℓ, lateral width b and thickness $w \ll \ell$ are held at a distance $D \ll \ell$ apart by a series of passive, linearly elastic cross-linker springs with areal density ρ_{N} and stiffness k_{N}. These structural features confer the composite with bending, shearing and extensional moduli. Specifically, as shown in the right upper tile, cross-linker springs are compliant in shear along the axial direction parametrized by the arc-length $s \in (0, \ell)$. We specify that these springs prevent any change in the gap thickness D; there are inextensible therefore in the lateral direction. Motivated by the high aspect ratio, slender filaments abundant in biology, we restrict ourselves to the limiting case $\ell \gg b \gg \max(w, D)$. Furthermore, to focus on the essential physics, we allow only for planar two-dimensional extensional, sliding and bending deformations of the composite filament. At length scales $\gg D$, the composite resists shear with an effective shear modulus that depends on D, ρ_N, and k_N. Suppose a shear stress σ_s acts upon the top filament with surface area $b\ell$, causing a sliding displacement Δ between both the filaments. This applied stress is balanced by the restoring elastic stress exerted by the connecting springs $\rho_{\mathrm{N}} b\ell$ leading to the force balance

relation, $\sigma_s b\ell \sim \Delta k_N \rho_N b\ell \sim G\Delta b\ell$. Th effective shear modulus of the whole strip that includes contributions from these passive springs is $G^* \sim D k_N \rho_N$ consistent with classical result for a passive cross-linked railway track model [*].

We next relate changes in the configuration as the composite deforms and decomposte the overall deformation into shear, slie and extensional parts. Consider two points $\mathbf{r}_1$ (on the upper strip, strip1) and $\mathbf{r}_2$ (on the lower strip, 2) that face each other when the composite is in the undeformed state. We define slide $\Delta(s)$ as difference between $\mathbf{r}_1$ and $\mathbf{r}_2$, relative to the initial pre-deformation value. Arbitrary deformations of the filament can be decomposed into three principal modes - bending, shear and stretching characterized by three scalar fields. The angle made by the tangent to the centerline, $\theta(s)$ is related to the slide $\Delta(s)$ and the displacement $u(s)$ by geometrical constraints. The local configurational geometry along the filament pair is defined by the relationships $d\mathbf{r}_1/ds = \mathbf{t}$, $d\mathbf{t}/ds = C\mathbf{n}$, and $d\mathbf{n}/ds = -C\mathbf{t}$. Here, $\mathbf{n}$ and $\mathbf{t}$ are the normal and tangent vectors at $\mathbf{r}_1$ (or equivalently at material point located at s), and $C = d\mathbf{t}/ds \cdot \mathbf{n} \approx d\theta/ds$ is the local curvature.

As the filament deforms, the location of $\mathbf{r}_2$ relative to $\mathbf{r}_1$ changes due to the deformation. We specify that the composite deforms such that the end at $s = 0$ is locally flat - i.e, we fix the tangent angle at $s = 0$ to be zero. Then using $(D + w)/\ell \ll 1$, we obtain to leading order

$$\mathbf{r}_2 - \mathbf{r}_1 \approx D\,\mathbf{n} + u\,\mathbf{t}, \tag{1}$$

$$\frac{d\mathbf{r}_2}{ds} \approx \mathbf{t} - D\,C\,\mathbf{t} + \frac{du}{ds}\,\mathbf{t} + u\,C\,\mathbf{n}. \tag{2}$$

which may be further simplified for small deformations satisfying $u\,C \approx 0$ in (2). Taking $|d\mathbf{r}_1/ds| = |\mathbf{t}| = 1$, we find $|d\mathbf{r}_2/ds| \approx 1 - D(d\theta/ds) + (du/ds)$. Finally, using the relation $d\Delta/ds = |(d\mathbf{r}_1/ds)| - |d\mathbf{r}_2/ds|$, then yields a simplified version of equation 2 that relates the spatial variation in the shear displacement to spatial variations in bending and stretching

$$\frac{d\Delta}{ds} = D\frac{d\theta}{ds} - \frac{du}{ds} \tag{3}$$

Integrating (3), and imposing the boundary condition $\theta(0) = 0$ yields the relationship between shear, extensional and bending deformations,

$$\Delta(s) = D\theta(s) - u(s). \tag{4}$$

We can define the energy functional per unit width E/b,

$$\frac{E}{b} = \frac{1}{2}\int_0^\ell \left(B_{\text{pas}} \left(\frac{d\theta}{ds}\right)^2 + K_{\text{pas}} \left(\frac{du}{ds}\right)^2 + G_{\text{pas}}\Delta^2 \right) ds. \tag{5}$$

Here, $B_{\text{pas}} \sim Ew^3$, $K_{\text{pas}} \sim Ew$ and $G_{\text{pas}} \sim \rho_N k_N$ are the passive bending, stretching and shear moduli, and E is the Young's modulus of the material. Since we have considered a strip like filament composite, these elastic properties of the composite we are to be interpreted as corresponding to a strip of unit width $b = 1$.

2.2 Euler-Lagrange equations provide static energy minimizing states

The Euler-Lagrange equations obtained by minimizing the functional (5) leads to force-balance relations that provide static solutions of a deformed filament, which we now derive in three limits.

1. **Persistence length for pure extension:** When the bending stiffness $B_{\text{pas}} \to \infty$, $d\theta/ds \to 0$ and the filament deforms due to shear and extension alone resulting in the constraint $\Delta \approx -u$. Minimization of (5) yields

$$\frac{d^2\Delta}{ds^2} - \left(\frac{G_{\text{pas}}}{K_{\text{pas}}}\right)\Delta = 0, \tag{6}$$

   which provides the relaxation length scale for pure extension $\ell_E^2 \equiv K_{\text{pas}}/G_{\text{pas}} \sim Ew/\rho_N k_N$.

2. **Persistence length for pure bending:** In the limit of inextensible filaments, $K_{\text{pas}} \to \infty$ and $du/ds \to 0$. Using the relation $\Delta \approx D\theta$ in this limit and minimizing (5) yields the equation

$$\frac{d^2\theta}{ds^2} - \left(\frac{D^2 G_{\text{pas}}}{B_{\text{pas}}}\right)\theta = 0, \tag{7}$$

   thus yielding the persistence scale for pure bending $\ell_B^2 \equiv B_{\text{pas}}/D^2 G_{\text{pas}} \sim Ew^3/D^2 k_N \rho_N$. Physically, this implies that as the density of passive links or their stiffness increases, the persistence length associated with purely bending modes decreases.

3. **Persistence length for general case:** Finally, we consider the general case when both bending and stretching modes are allowed. Allowing for sliding deformations at $s = 0$, we repeat the minimization procedure to obtain the two coupled equations,

$$B_{\rm pas}\frac{d^2\theta}{ds^2} + DK_{\rm pas}\left(D\frac{d^2\theta}{ds^2} - \frac{d^2\Delta}{ds^2}\right) = 0, \quad \text{and} \quad K_{\rm pas}\left(\frac{d^2\Delta}{ds^2} - D\frac{d^2\theta}{ds^2}\right) - G_{\rm pas}\Delta = 0 \tag{8}$$

corresponding to $\delta E_T/\delta\theta = 0$ and $\delta E_T/\delta\Delta = 0$ respectively. Eliminating θ from the pair of equations in (8) we find,

$$\frac{d^2\Delta}{ds^2} - \frac{\Delta}{\ell_*^2} = 0 \quad \text{with} \quad \ell_* \equiv \frac{\ell_B\ell_E}{\sqrt{\ell_B^2+\ell_E^2}} \sim \left[\frac{w/D}{\sqrt{1+w^2/D^2}}\right]\left(\frac{K_{\rm pas}}{G_{\rm pas}}\right)^{\frac{1}{2}} \tag{9}$$

Thus variations in the sliding displacement Δ are associated with a persistence (decay) length ℓ_* (equation (9)) that depends on geometrical properties and elastic properties. Referring back to Figure 2, we note that increasing either the density of the passive springs (red) or their stiffness leads to increased shear resistance of the composite filament. This effectively renormalizes the bending modulus and the extensional modulus. Composites made of filaments that are each extremely stiff and resist extension (such as microtubules) may ultimately be forced to extend deform in the presence of cross-linkers that connect them and generate very high shear resistances. The generality of the framework suggests that similar length scales should appear in a variety of soft systems where bending, shear and extension are coupled, as indeed has been observed more than 75 years ago in both microscopic and macroscopic contexts (38, 39).

To put the discussion in perspective, we consider typical parameters for a canonical ordered active composite - the axoneme seen in sperm flagella. We take w and D as the radius and the spacing of microtubules, E as the Young's modulus of microtubules, $k_{\rm N}$ as the stiffness of passive (nexin) links and $\rho_{\rm N}$ as the density of these links. Using $w \sim 20$ nm, $D \sim 40$ nm (12), $E \sim 1.2$ GPa (3, 12), $k_{\rm N} \sim 16-100$ pN μm^{-1} (40) and $w\rho_{\rm N} \sim 10^5 - 10^7$ m^{-1} (40, 41), we estimate $\ell_E \sim 200-500$ μm while $\ell_* \sim 80-200$ μm. This estimate is however with just the passive cross linkers contributing to the shear stiffness and therefore values should be treated as an upper limit. Motor activity will naturally influence this scale as attached motors contribute to the instantaneous shear resistance. Assuming that all motors are bound, with linear density $O(10^8)$ m^{-1} and effective spring stiffness of 10^{-3} N/m, we obtain $\ell_E \sim 5-10$ μm. Since sperm flagella are often much longer than this scale (3), the role played by activity in modulating persistence lengths can be crucial and important.

3 MEAN-FIELD MODEL FOR ACTIVE ASSEMBLIES: WEAKLY ELASTIC SYSTEMS AND LOW NOISE

Having analyzed the decay length in a model passive composite assembly, we now move to the case of active assemblies. The composite we analyze here in the mean-field model is illustrated in the lower right tile of Figure 2. The system comprises of two cross-linked sheets (with unit width) as in the passive case that are held together a distance D apart by passive springs that are compliant in shear but resist normal deformations. We simplify the system further by specifying that only the upper filament is extensible; the lower filament is assumed to be rigid and static. Our focus is on the competition between shear and extension in setting decay lengths; bending modes are thus ignored in further analysis. Additionally, the gap spanning the filaments is populated by arrayed molecular motors that are grafted to the lower surface and are distributed homogeneously along s with constant density ρ_m. The action of these motors is to generate an active force $F_m(s)$ (per unit width) - this force comes from motors periodically attaching to the upper strip surface and exerting tangential forces on the upper strip. We treat the active motors as unidirectional motors interacting with the potential generated by the upper strip. Finally, we consider the biological relevant limits with inter-link (passive links) spacing and inter-motor (active links) spacing much smaller than the filament length. Now when $b \gg \max(w, D)$, a continuum, one-dimensional description of the passively cross-linked, motor-filament aggregate is appropriate.

3.1 Force balance relates extensional deformation of composite assembly to active forces

We consider next a model that incorporates mechanical properties of each motor and specifies the manner in which attached motors interact with the upper filament. Following previous work, we specify that each attached active motor behaves elastically as an active linear spring (9, 10) with spring constant k_m and zero rest length. The internal mechanical state of the motor is characterized by a single internal variable – its extension $y(s,t)$. The motor extension serves as an indicator of how much the head of the motor is displaced relative to the tail (appropriately measured from a rest state). Motors attach in a pre-strained state with an (initial) extension d_m. Once attached, in order to relax the pre-stress, the head *convects as well as slides relative to the filament* (thus working against an effective filament-motor interaction potential) with a motor-strain dependent speed, resulting

in a changing motor extension $y(s,t) \neq d_m$. The motor of the motor head in the interaction potential field generates an effective active force. We ignore Brownian diffusion of both the motor base and the motor head. Thus the net active force arises from both the initial configuration of the motors just as they attach (and thus pre-straining the internal linear spring), and the forces generated subsequently as the motor heads slide along the filament. Attached motors undergo a conformational change with strain (extension) given by

$$\partial y/\partial t = -\partial u/\partial t + v_o(1 - k_m y/F_s)$$

where v_o is the maximum (zero-load) velocity of the motor and F_s is the stall force. The intrinsic extension y of each motor can take positive as well as negative values. We now focus on an infinitesimal length between s and $s + ds$ of the filament and averaging over forces exerted by all motors. Let a fraction N of total motors be attached over this small segment. The averaged active force per motor F_m, is related to ρ_m and the averaged stretch $\langle y \rangle$ (averaged over all motors - attached and detached) by

$$F_m = k_m N \langle y \rangle. \tag{10}$$

In the biologically relevant over-damped limit, inertial effects are not important. Ignoring bending deformations, a force balance provides the equation for the strain field $u(s,t)$

$$K_{\text{pas}} \frac{\partial^2 u}{\partial s^2} - G_{\text{pas}} u + \rho_m F_m = 0. \tag{11}$$

In equation (11), motor activity is treated as an internally distributed force density per motor. We note that F_m and $\langle y \rangle$ are both functions of s and of t. In the absence of activity $F_m = 0$, equation (11) predicts that local perturbations in the extensional strain u decay exponentially with a length scale $\ell_E \equiv \sqrt{K_{\text{pas}}/G_{\text{pas}}} = \sqrt{Ew/\rho_{\text{N}} k_{\text{N}}}$.

At high motor densities, the number of attached motors is large and temporal fluctuations in the density of attached motors $\rho_a(s,t) = \rho_m N(s,t)$ are small compared to the mean value. Motor kinetics may then be described using population balances. The balance equations relating attached and detached probability densities $\mathcal{P}_a(s,y,t)$ and $\mathcal{P}_d(s,y,t)$ respectively, to attachment and detachment fluxes J_a and J_d via attachment and detachment transition rates $\nu_{\text{on}}(y)$ and $\nu_{\text{off}}(y)$ respectively are

$$\frac{\partial \mathcal{P}_a}{\partial t} + \frac{\partial J_a}{\partial y} = \nu_{\text{on}} \mathcal{P}_d - \nu_{\text{off}} \mathcal{P}_a, \tag{12}$$

$$\frac{\partial \mathcal{P}_d}{\partial t} + \frac{\partial J_d}{\partial y} = \nu_{\text{off}} \mathcal{P}_a - \nu_{\text{on}} \mathcal{P}_d. \tag{13}$$

To make analytical progress, we treat ν_{on} in (12) and (13) as constant. Detachment probabilities are allowed to depend on y, with $\nu_{\text{off}} = \nu_{\text{off}}(y, \delta_m)$. Here, δ_m is the typical extension at which the detachment rate becomes significant.

A series of simplifications allow us to reduce equations (12) and (13) further. First we specify that detached motors rapidly relax to an equilibrium state with zero motor extension and with mean detached density ρ_d. This implicitly assumes a dissipative component to the motor kinetics as stored elastic energy is lost in this process. Second, we specify that the value of y for attached motors is sharply peaked about an average extension; variations are assumed to occurring over negligibly small time scales. This implies that $\mathcal{P}_a = \rho_a(t)\delta(y - \langle y \rangle)$ where δ here is the Dirac delta function. The mean value of a motor state dependent variable X is then obtained via $\int X \mathcal{P}_a dy \equiv \langle X \rangle N \rho_m$. Using $\mathcal{P}_a$ we integrate equations (12) and (13). In the process, microscopic probabilities (attachment and detachment) are ensemble averaged to obtain the mean-field attachment rate ω^0_{on}, and the mean field detachment rate, $\langle \nu_{\text{off}} \rangle = \omega_{\text{off}}$. The final zeroth moment equation is

$$\frac{\partial \rho_a}{\partial t} = \omega^0_{\text{on}} \rho_m - \rho_a(\omega^0_{\text{on}} + \omega_{\text{off}}(\langle y \rangle)). \tag{14}$$

The quantity $\mathcal{E} \equiv k_m \delta_m^2 / k_B T$ provides a measure of the energy needed to stretch the motors and cause them to detach. Based on this picture that invokes strain-based (energy based) detachment rate we set $\omega_{\text{off}} = \omega^0_{\text{off}} \mathcal{F}(\mathcal{E}, Y)$. For slip bonds, $\mathcal{F}(\mathcal{E}, Y)$ increases monotonically with Y. While we choose two specific forms to present results - $\cosh(\mathcal{E}Y)$ and $\exp(\mathcal{E}Y)$ - other functional forms yield similar results. To obtain the mean motor extension $\langle y \rangle$ we multiply (13) by y and then integrate over all y

$$\frac{\partial \langle y \rangle}{\partial t} = -\langle \nu_{\text{off}}\, y \rangle - \frac{\partial u}{\partial t} + v_o \left(1 - \frac{k_m y}{F_s}\right) + \langle \nu_{\text{off}} \rangle \langle y \rangle + \omega^0_{\text{on}}(d_m - \langle y \rangle) \left(\frac{1 - N}{N}\right). \tag{15}$$

Using $\langle \nu_{\text{off}}\, y \rangle \approx \langle \nu_{\text{off}} \rangle \langle y \rangle$, we obtain

$$\frac{\partial \langle y \rangle}{\partial t} = -\frac{\partial u}{\partial t} + v_o \left(1 - \frac{k_m y}{F_s}\right) + \omega^0_{\text{on}}(d_m - \langle y \rangle) \left(\frac{1 - N}{N}\right). \tag{16}$$

Symbol	Definition	Interpretation
G_{pas}	$\rho_{\text{N}} k_{\text{N}}$	Passive shear modulus
K_{pas}	Ew	Extensional modulus
G_{act}	$\rho_m k_m$	Active shear modulus
ω_{on}		Ensemble averaged motor attachment rate
ω_{on}^0		Motor attachment rate at zero load
ω_{off}		Ensemble averaged motor detachment rate
ω_{off}^0		Motor detachment rate at zero load
$\rho_a(s,t)$		Density of attached motors at position s
$\langle y \rangle(s,t)$		Ensemble averaged (mean) motor extension at position s
$u(s,t)$		Filament elongation (extensional strain)
$\mathcal{A}_1$	$v_o k_m/(\omega_{\text{off}}^o F_s)$	Scaled active velocity
$\mathcal{A}_2$	$F_s/(k_m \delta_m)$	Scaled active force
$\mathcal{A}_3$	d_m/δ_m	Scaled active displacement
$\mathcal{E}$	$k_m \delta_m^2/k_B T$	Scaled energy scale for detachment
Ψ	$\omega_{\text{off}}^o/\omega_{\text{on}}^o$	Scaled duty ratio
$N(s,t)$	ρ_a/ρ_m	Ensemble averaged fraction of total motors attached
$Y(s,t)$	$\langle y \rangle/d_m$	Ensemble averaged (mean) motor extension
$U(s,t)$	$u(s,t)/d_m$	Scaled filament extension (strain)

Table 1: Variables and parameters that appear in the mean-field model. In the first column, symbols in blue indicate dimensional parameters and variables while symbols in black are dimensionless.

In equation (16), the first term on the right hand side is the stretch due to the passive motion of the attached motor, the second term gives the motor velocity relative to the filament, and the third term (in black) corresponds to the rate at which the mean strain changes due to the kinetics of motor attachment and arises from the difference in extension of attaching and detaching motors.

3.2 Dimensionless equations and parameters

We next proceed to simplify (14) and (16) to derive dimensionless forms of these equations and in the process identify important dimensionless parameters. Scaling time with $(\omega_{\text{on}}^0)^{-1}$ and setting $\rho_a(s,t) = \rho_m N(s,t)$, equation (14) may be recast as

$$\frac{\partial N}{\partial t} = (1 - N) - \Psi \mathcal{F}(\mathcal{E}, Y) N \tag{17}$$

where the dimensionless number $\Psi \equiv \omega_{\text{off}}^0/\omega_{\text{on}}^0$ is dependent on the duty ratio of the motors. Defining $U \equiv u/\delta_m$, equation (16) becomes

$$\frac{\partial Y}{\partial t} = -\frac{\partial U}{\partial t} + \mathcal{A}_1 \Psi \left(\mathcal{A}_2 - Y\right) + \left(\mathcal{A}_3 - Y\right)\left(\frac{1-N}{N}\right). \tag{18}$$

Combining (10) and (11), we set $\bar{s} = s/\sqrt{K_{\text{pas}}/G_{\text{pas}}}$ to obtain

$$\frac{\partial^2 U}{\partial \bar{s}^2} - U + \beta N Y = 0, \quad \text{where} \quad \beta \equiv G_{\text{act}}/G_{\text{pas}} \quad \text{and} \quad G_{\text{act}} = \rho_m k_m. \tag{19}$$

Here, G_{act} is the active analogue of the passive shear modulus. Equations (17)-(19) constitute our mean-field model. We note that the set involves four dimensionless parameters that depend purely on the motor kinetics: (1) $\mathcal{A}_1 \equiv v_o k_m/(\omega_{\text{off}}^o F_s)$, (2) $\mathcal{A}_2 \equiv F_s/(k_m \delta_m)$, (3) $\mathcal{A}_3 \equiv d_m/\delta_m$, and (4) $\Psi \equiv \omega_{\text{off}}^o/\omega_{\text{on}}^o$. Table 1 provides a physical interpretation of these dimensionless parameters. To find steady homogeneous solutions (N_0, Y_0, U_0) that are independent of both space $\bar{s}$ and time t, we set $\partial U/\partial t = \partial Y/\partial t = \partial N/\partial t = 0$ in (17)-(19) to obtain

$$(N_0, Y_0, U_0) = \left(\frac{1}{1 + \Psi \mathcal{F}_0}, \quad \frac{\mathcal{A}_1 \mathcal{A}_2 + \mathcal{A}_3 \mathcal{F}_0}{\mathcal{A}_1 + \mathcal{F}_0}, \quad \beta N_0 Y_0\right), \quad \mathcal{F}_0 \equiv \mathcal{F}\left(\mathcal{E}, Y_0\right). \tag{20}$$

Our mean-field approach and analysis leading to equations (17)-(19) complements and differs from previous attempts in a few important ways. First, consistent with experiments suggesting that bond failure is more naturally dependent on the extension and only weakly on the rate of extension, we have chosen ω_{off}^o to depend on motor extension (9, 10) and not the rate of extension (42). Second, non-linear coupling between passive and active deformations in (17)-(19) distinguishes our model from previous studies of motor mediated bending of filaments (42). Finally, our model filament is weakly extensible, bolstered

by recent experimental evidence (3, 7, 37). Equation (19) ignores passive viscous drag on the deforming filament due to any external fluid resistances. This may be incorporated into equation (11) by adding a term $-\mathcal{A}_4\ (\partial U/\partial t)$ on the left side of the equation proportional to the external viscosity. (see ESM Sections 1 and). We find that external viscous resistances does not change results qualitatively.

3.3 Persistence length for assemblies in rigor

When the motors are in a state of rigor, they are stuck in fixed configurations (either attached or detached). Therefore we may set $\omega^0_{\rm on} = 0$, $\omega^0_{\rm off} = 0$ and $v_o = 0$. Attached motors are permanently bound to the filament track and can sense the instantaneous displacement of the attachment point (where the head is) rather than just the rate of displacement. The number of attached motors N_R cannot change and may differ from N_0. The motor extension Y responds passively to any changes in the attachment point of the motor head, so that (18) simplifies to:

$$\frac{\partial Y}{\partial t} = -\frac{\partial U}{\partial t}. \tag{21}$$

Integrating the above equation once yields

$$(Y(\bar{s},t) - Y(\bar{s},0)) = -(U(\bar{s},t) - U(\bar{s},0)). \tag{22}$$

Since $U(\bar{s},t) - U(\bar{s},0) = \delta U$ the filament strain, we have

$$\frac{\partial^2 U}{\partial \bar{s}^2} - \delta U(1 + \beta\, N_R) = 0. \tag{23}$$

While equation (23) can be solved numerically subject to appropriate boundary conditions for arbitrary spatially varying N_R, insight may be gained by looking at the case where N_R is uniform and independent of s. Matching magnitudes of the two terms, we then obtain the characteristic length scale $\lambda_{\rm R}$ over which the strain decays in this rigor state

$$\lambda_{\rm R} = \sqrt{\frac{K_{\rm pas}/G_{\rm pas}}{\beta\, N_R + 1}} = \sqrt{\frac{K_{\rm pas}}{k_m \rho_m N_R + G_{\rm pas}}}. \tag{24}$$

The effective shear modulus due to the links, $G_{\rm eff}$ is obtained by equating the force needed to shear the composite - here, the motor springs act as passive springs. This procedure yields $(N_R \rho_m k_m + \rho_N k_N)(ds\ b)\langle y\rangle = F_s = G_{\rm eff}(\langle y\rangle/D) ds\ b$, thus yielding an estimate for the effective modulus

$$G_{\rm eff} \sim (N_R \rho_m k_m + \rho_{\rm N} k_{\rm N}) D. \tag{25}$$

Equations (24) and (25) are relevant to the onset of beating from an inactivated or rigor state in filament-motor assembles. Since $0 \le N_R \le 1$ and hence λ_R has an upper and lower bound for composite filaments in rigor. When $\rho_m N_R > (\rho_N k_N/k_m)$ motors dominate and control the shear modulus. A spatially varying N_R implies spatial variational shear modulus and spatially varying persistence lengths.

3.4 Persistence lengths for active assemblies

The homogeneous and stationary base state, equation (20), is susceptible to perturbations and depending on the values of $N_0, Y_0, U_0, \mathcal{F}_0$ and $\mathcal{F}_0' \equiv (d\mathcal{F}/dY)_{(\mathcal{E},Y_0)}$, may be linearly stable or unstable. For stable solutions, the base state further determines the effective extensional and shear moduli and determine the persistence lengths of strain fields. We therefore next analyze equations (17)-(19) about the base state (20) to derive analytical expressions for the persistence lengths associated with imposed or emergent steady strains, as well as with imposed oscillatory strain fields.

3.4.1 Localized strains and emergent oscillations

Before we study the strain field in the full extensible filament, we first examine the stability of the stationary solutions and seek conditions under which oscillations may spontaneously onset. To further examine how inhomogeneities in motor properties may trigger these instabilities, we study a specific model system. We choose a small internal part (segment) of the composite filament of with length $\ell_s \ll \sqrt{K_{\rm pas}/G_{\rm pas}}$. In this limit, we can ignore the extensibility of the segment and study local dynamics as it interacts elastically with its neighboring domains. Such a description is also relevant to the dynamics of small local stiff regions of the composite filament starting from a rigor state when N_R is spatially varying and the composite is comprised of

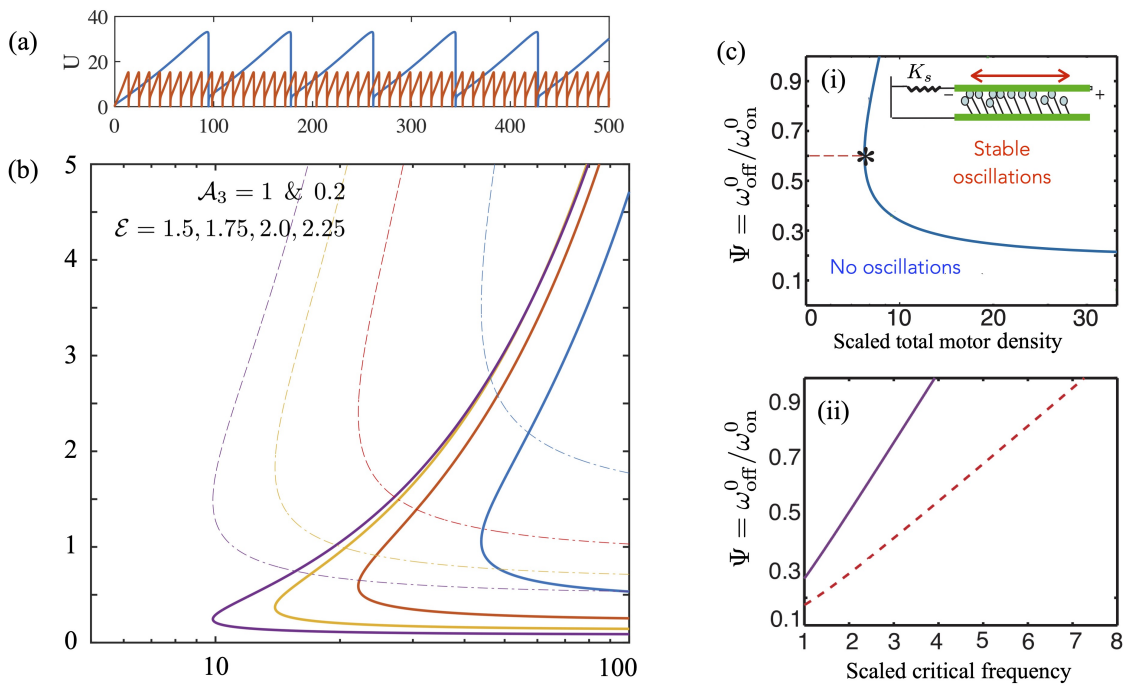

Figure 3: Mean field results for the dynamics of a small rigid interior segment driven by motors and working against a resisting spring in the absence of external fluid drag. (a) Sample oscillations observed in the limit of vanishing external viscosity indicating that external viscosity acts as a regular perturbation to the equations. Zero viscosity solutions have the same forms as shown here (see also ESM Figure-3). The red curves correspond to $\Psi = 0.3$ while the red curves correspond to $\Psi = 1.0$. The activity parameter $\beta = 100$, $\mathcal{A}_3 = 1.0$, $Y_0 = \mathcal{A}_3$, $\mathcal{A}_4 = 10^{-4}$, and the detachment function $\mathcal{F} = \exp(2Y)$. (b) Neutral stability curves for the case where there is no fluid drag: $\mathcal{A}_4 = 0$ and $\mathcal{A}_1 = 0$. here. The detachment function shown is $\mathcal{F} = \exp(\mathcal{E}|Y|)$. The curves correspond (from top to bottom) to $\mathcal{E} = 1.5, 1.75, 2.0$ and 2.25. Solid curves correspond to $\mathcal{A}_3 = 1$ while dash-dot curves correspond to $\mathcal{A}_3 = 0.2$. (c) (i) Focussing on one value of $\mathcal{E}$, we show the neutral stability curve $\Psi = \omega^0_{\rm off}/\omega^0_{\rm on}$ vs. scaled density of motors, $\rho_m k_m/K_s$ for $\mathcal{E} = 4.944$, $Y_o = 0.5$ and $\omega^0_{\rm on} = 0.25$ s^{-1}. For fixed Ψ, there is a critical number of motors required for oscillations to manifest (the value for $\Psi = 0.6$ is indicated as an example. (ii) Scaled frequency of oscillations, $\omega_c/\omega^0_{\rm on}$ as a function of Ψ. The solid line is the exact result while the dashed line is the adiabatic approximation where motor extension is slaved to the filament dynamics (see ESM §1).

stiff regions surrounded by relatively soft regions. The dynamics of this segment relative to its neighbors can be mapped to that of a homogeneous population of motors acting on a rigid segment (see ESM-§I and in ESM Figures 1-3) and working against an external spring with effective stiffness K_s with active and passive components. The active contribution comes from attached motors in neighboring filaments, and the passive contributions from k_N and Ew. If $\rho_N = 0$ then the passive part of $K_s \propto K$. Since the fragment is inextensible, the force balance equations (11) and (19) become

$$-U + \frac{\rho_m k_m}{K_s} NY = 0 \tag{26}$$

For $K_s > 0$, a globally translating solution ($U > 0$ and constant) is not possible but oscillatory solutions can exist. To discern the existence of such solutions, we analyze the linear stability of the base state (20) to infinitesimal perturbations. Setting $N = N_0 + N_1 e^{\sigma t}$, $Y = Y_0 + Y_1 e^{\sigma t}$ and $U = U_0 + U_1 e^{\sigma t}$ where N_1, Y_1 and U_1 are small quantities, we first linearize equations (17)-(19).

Recasting these equations in matrix form, we evaluate constraints on the matrix for non trivial solutions and study associated eigenspectrum and variations of growth rate σ. We find the existence of stable oscillations (limit cycles) for certain values of the parameters. These emergent actively driven oscillatory states bifurcate with well-defined frequencies from the stationary state via Hopf-Andronov-Poincare bifurcations. In all cases, we find that stable oscillatory solutions exist only within a range of Ψ values. Furthermore, studying the eigenvalues of the linearized equations provides insight into the origin of the oscillations – we find that oscillations are driven by positive feedback - i.e, the emergence of negative effective spring constants and/or

negative friction coefficients characterizing the motion of the filament. In turn, these negative coefficients arise to the interplay between the motor kinetics and filament. For large values of Ψ, the number of attached motors is insufficient to supply the energy for oscillations thus suggesting an upper bound. For small Ψ, too many attached motors increase the net elastic resistance and friction coefficients, causing a strong damping of oscillations. In the stable oscillating state, the active energy input to the system by active motors attaching balances the effective irreversible viscous dissipation due to motor friction as motors detach. Numerical exploration of the stability boundary for one set of parameter values (with $\mathcal{A}_1 = 0$, and $\mathcal{A}_3 = 1$) may be seen in in Figure 3(a). The neutral stability curve is seen to depend on Ψ, $\mathcal{E}$ and β. Figure 3(b) shows the correlation between the dimensionless frequency at onset ω_c as a function of Ψ. Details on the linearization process, analytical expressions for the stability boundary separating stationary and oscillatory states, and for the emergent frequencies may be found in ESM §1 and ESM Figure 1-3.

3.4.2 Persistence length for steady extensional strains is independent of activity

Our analysis in §3.5.1 demonstrates that localized steady, or oscillatory extensional strains may spontaneously emerge in a small fragment of a larger active composite. For a filament with infinite elastic modulus $K_{\text{pas}} \to \infty$, the effect of localized strains is felt everywhere along the filament; this enables spatially separated motor groups to synchronize and behave coherently.

Starting from this limit of perfect coherence, we next analyze how elasticity modulates the decay of strains, introduces a persistence length and disrupts coherence. We begin by identifying the appropriate base state that sets the strain field over the length of the composite filament. The stationary fields (U_0, N_0, Y_0) are solutions to

$$\frac{d^2 U_0}{d\bar{s}^2} - U_0 + \beta\, N_0 Y_0 = 0. \tag{27}$$

We next choose boundary conditions consistent with the end corresponding to $\bar{s} = 0$ held fixed so that $U_0(0) = 0$. The free end $\bar{s} = \ell/\ell_E$ satisfies the force-free condition $(dU_0/d\bar{s})_{(s=\ell/\ell_E)} = 0$. Solving equation (27) with these boundary conditions, we find

$$U_0(\bar{s}) = \beta\, N_0 Y_0 \left(1 - \alpha\, e^{\bar{s}} - (1-\alpha)\; e^{-\bar{s}}\right), \quad \alpha \equiv e^{-2\ell/\ell_E}(1 + e^{-2\ell/\ell_E})^{-1}. \tag{28}$$

The strain U_0 is thus linear in β; the decay length is however *independent of* β. This surprising result may be rationalized as follows. Attached motors sense the strain rates of the filament but they do not have any way to gauge the amplitude (magnitude) strain at the point of attachment at the time of attachment or later. The passive linkers on the other hand sense both the absolute strain as well as strain rates since, unlike active motors, they serve as permanent links. In the absence of any time dependence, the decay length of steady *extensional strains* can only depend on the passive constituents of elasticity.

3.4.3 Motor activity results in strain softening and determines frequency dependent persistence lengths and ability to synchronize

We next ask how localized oscillatory extensional strains decay with distance from the point of localization. This question is naturally related to the emergence of coherent dynamics between spatially separated motor domains, each having its own dynamical response. Specifically, this is related to the conditions under which two spatially separated oscillating motor aggregates, lock into synchronous oscillations due to strains transmitted by an elastic connecting filament. To study this limit, we modify the boundary condition at $s = \ell$ in a manner that enables oscillations there, while still respecting the constraints that lead to (28). This is achieved by subjecting the free end to an imposed oscillatory displacement with frequency ω and small amplitude $\epsilon \ll \max|U_0|$. These conditions ensure that the base state that is being probed is stationary and stable. The boundary conditions then take the form $U(0,t) = 0$ and $U(\ell,t) = U_0(\ell) + \epsilon \text{Real}(e^{i\omega t})$.

Analytical progress is possible if we focus on the frequency-locked homeostatic response where the imposition of oscillatory displacement with frequency ω at the free end results in the strain field and both motor-related variables responding at the same frequency. In this scenario, we can write $(U, N, Y) = (U_0, N_0, Y_0) + \epsilon e^{i\omega t}(\hat{U}, \hat{N}, \hat{Y}) + O(\epsilon^2)$. Substituting this in equations (17)-(19), then expanding and retaining terms through $O(\epsilon)$ we obtain

$$K_{\text{pas}}\, \partial_{ss}\hat{U} - G_{\text{pas}}\hat{U} - G_{\text{act}}\chi\hat{U} = 0. \tag{29}$$

The boundary conditions are also expanded to $O(\epsilon)$ consistent with the linearization that lead to (29). The compliance function $\chi = -(N_0\hat{Y} + Y_0\hat{N})/\hat{U}$ determines the linear compliance of the motors-linker system.

In ESM §2.1, we explore the solution to (29) for finite ℓ that includes the effects of finite filament length. Equations (17) and (18) of the ESM provide the exact solution to the strain field for arbitrary values of ℓ/ℓ_E. In general, the solution has to be obtained by consideration of the complex values of χ. To extract the delay length for localized imposed oscillatory strains, it is

easiest to work with (29) and study the limiting behavior of solutions for long filament lengths. We define variable $x = (\ell - s)$ so that equation (29) may be written as

$$\ell_E^2 \partial_{xx} \hat{U} = (1 + \beta\chi)\hat{U} \tag{30}$$

with boundary conditions $\hat{U}(x = 0) = 1$ and $\hat{U}(x = \ell/\ell_E) = 0$. Assuming solutions of the form $\hat{U} = \hat{U}_* \exp(-x/\lambda)$ provides the equation $\ell_E^2 = \lambda^2(1 + \beta\chi)$. Note that, in principle, one may choose very large ℓ such that $\ell/\ell_E \to \infty$ consistent with exponentially decaying solutions. Analysis of (29) described in ESM § 2.2 suggests that there exists a cross-over value for G_{pas} separating the regime where the decay length is dominated by active motor properties from the regime where passive linker-derived elasticity controls the variations of the strain field. We define the decay length scale λ_E via the relationship

$$\lambda_E \equiv \sqrt{2\frac{K_{\text{pas}}}{G_{\text{act}}}} \left[\text{Real} \left(\sqrt{\frac{1}{2\beta^{-1} + 2\chi}} \right) \right]. \tag{31}$$

For $G_{\text{pas}} = 0$ as in our simulations, the parameter $\beta^{-1} = 0$, and simplifying (31) provides

$$\lambda_E(G_{\text{pas}} = 0) = \sqrt{2\frac{K_{\text{pas}}}{G_{\text{act}}}} \left(\frac{|\chi| + \text{Real}(\chi)}{4|\chi|} \right)^{\frac{1}{2}}. \tag{32}$$

Note that the blue part of the right hand side is frequency independent while the red part depends on the frequency ω.

4 BROWNIAN-MPC SIMULATIONS OF COMPOSITE FILAMENTS

Having studied the role of shear stiffness due to passive links in controlling the bending and extension of deformed filaments, we now describe our discrete, microscopic model that includes noise due to motor activity. This allows us to achieve two objectives. First, we can qualitatively compare the influence of noise in systems containing filaments and motors by selecting a finite number of motors and second, we can adjust the discrete version of the filament elasticity K_{pas} and study stiff, moderate as well as soft filaments. The latter two regimes are inaccessible to the mean-field theory.

4.1 Discrete model for noisy systems

The discrete analog of the weakly extensible filament is modeled as a one dimensional chain of M rigid segments (the unit cell is illustrated in the inset in Figure 3(a) and the complete composite filament in Figure 5(a)). Each segment has length $\ell_s = 80\,\sigma$, and is made up of M_m discrete spherical monomers of diameter σ located at r_i, $(i = 1, ..., N_m)$. The monomers are connected by the elastic potential below that controls the stretchability within each segment

$$u_s = \frac{\kappa_s}{2} \sum_{i=1}^{M_m - 1} \left(|\mathbf{r}_{i+1} - \mathbf{r}_i| - \sigma \right)^2. \tag{33}$$

Each segment is also connected to neighboring segments by linear elastic spring of stiffness $\propto K_{\text{pas}}$ (the proportionality constant being dependent on σ/ℓ) with rest length 80σ. With $\ell \gg \ell_s$ since $M \gg 1$, bending and extensional deformations can be ignored within each segment. The first segment is connected to a rigid wall by the same elastic potential at location corresponding to $s = 0$ while the other end of the composite at $s = \ell$ is kept free. Bending stiffness is implemented via a three-body bending potential

$$u_{\text{b}} = \frac{\kappa}{2\sigma} \sum_{i=2}^{M_m - 1} (\mathbf{t}_{i+1} - \mathbf{t}_i)^2 \tag{34}$$

where $\mathbf{t}_i = (\mathbf{r}_i - \mathbf{r}_{i-1})/|\mathbf{r}_i - \mathbf{r}_{i-1}|$. The effective bending rigidity κ penalizes angular changes from a local straight geometry for the segments. In our simulations $\kappa_s = 2 \times 10^4 \left(k_B T/\sigma^2\right)$ and $\kappa/\sigma = 2 \times 10^4 \left(k_B T\right)$ with an appropriately large persistence length for the segment $\sim 250\,\ell_s$. While our model is general enough to include bending deformations by treating κ as a variable parameter - here we focus solely on extensional strain on the filament.

Motors that impose active forces that cause filament shear and extension are modeled as linear elastic springs with stiffness k_m and rest length ℓ_m. These motors are uniformly distributed on each segment with number density ρ_m. One end of the motor (tail) is grafted to a point $\mathbf{r}_t$ on a rigid base while the other end (head) can attach and detach to a given monomer, located at $\mathbf{r}_h$, of the filament. During the attachment process, the monomer bead which lies closest to the motor head is chosen so that the motor extension, $|\mathbf{r}_h - \mathbf{r}_t| - \ell_m$, upon attachment is minimal. Similar to the mean-field model, we assume a constant attachment

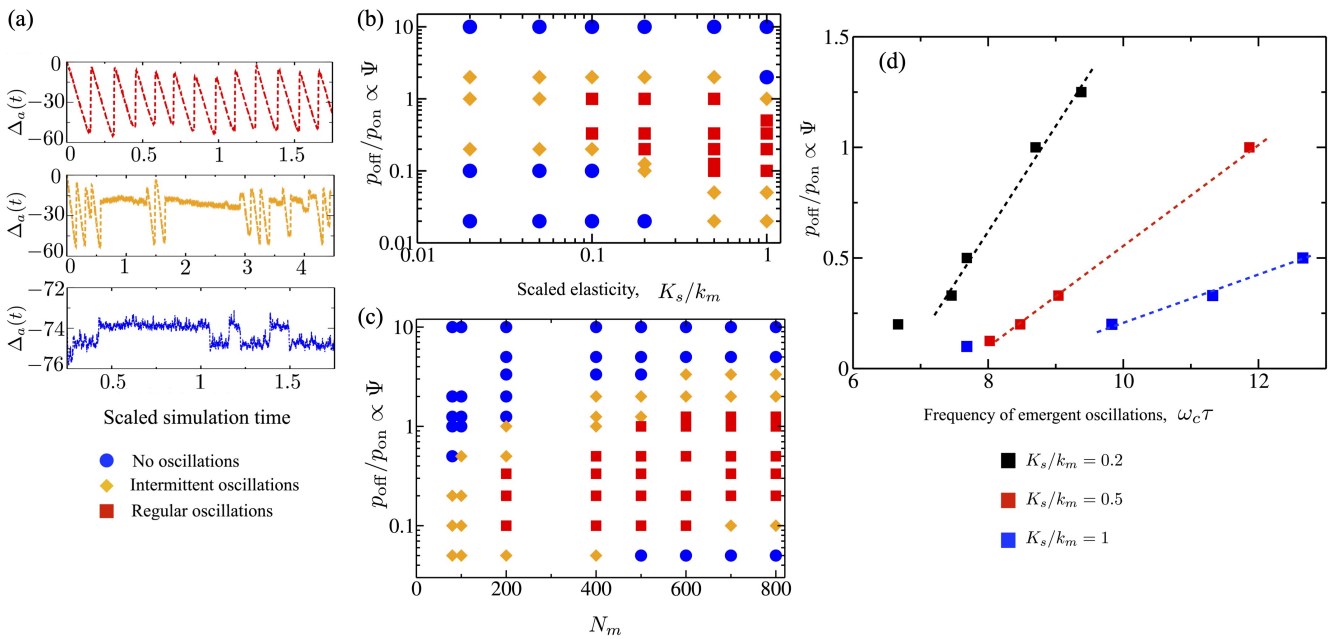

Figure 4: (a) The time dependent displacement of the free end, $\Delta_a(t)/\sigma$ for a fixed value $K_s/k_m = 0.2$, and for zero load motor detachment/attachment probabilities, $p_{\text{off}}/p_{\text{on}} = 1.0$ (top), 2 (middle) and 10 (bottom), illustrating various dynamical regimes observed in simulations. Phase diagram from the Brownian-MPC simulations indicating the dynamical regimes as a function of (b) the number (density) of total motors acting on the segment and (c) of the ratio K_s/k_m. The plots show how the stability boundary is influenced by $p_{\text{off}}/p_{\text{on}}$. The observed dynamical regimes are, steady extension (blue, circle), intermittent oscillations (orange, diamonds), and steady oscillations (red, squares). Colored regions are a guide to the eye. (d) The oscillation frequency of a periodically oscillating filament also obtained from the Brownian-MPC simulations with $K_s/k_m = 0.5$.

probability p_{on} for each motors. Once attached, the unidirectional motor head steps to the next monomer in the direction of the anchored end, $s = 0$, with a discrete step size that equals the monomer diameter a. As the motor heads move, the accompanying extension of the motor length leads to a force $\mathbf{F}_m = -\kappa_m(|\mathbf{r}_h - \mathbf{r}_t| - \ell_m)\,\hat{\mathbf{e}}$, where the unit vector $\hat{\mathbf{e}} = (\mathbf{r}_h - \mathbf{r}_t)/|\mathbf{r}_h - \mathbf{r}_t|$, that acts on the attached filament. This force is balanced by the tension on the filament to which the motor is attached, thus resulting in a localized active strain on the filament. We assume a load dependent stepping velocity of the motor head, choosing a linear relationship, $v_h = v_o(1 - |\mathbf{F}_m|/f_{\text{max}})$ with f_{max} being the stall force F_s consistent with the form assumed in the mean-field theory. Motor heads that are attached to the filament sense the load and detach at a rate given by the load dependent probability $\tilde{p}_{\text{off}}$, defined by the piecewise function

$$\tilde{p}_{\text{off}} = \begin{cases} p_{\text{off}}, & \text{if } |\mathbf{F}_m| \le f_{\text{cut}} \\ 1, & \text{if } |\mathbf{F}_m| > f_{\text{cut}}, \end{cases} \tag{35}$$

where p_{off} is the load independent detachment rate of motors and f_{cut} is the motor cut-off load. We take $f_{\text{cut}} = f_{\text{max}}$ in our simulations, although in general they are not necessarily equal.

The load dependence of the detachment probability of individual motors allows for the crucial two-way coupling between filament elasticity and the motor response and also sets the critical motor extension at which detachment occurs. Furthermore, the constant load independent detachment probability p_{off} in conjunction with p_{on} yields an equilibrium fraction of attached motors, $p_{\text{on}}/(p_{on} + p_{\text{off}})$. We recall that in the continuum theory, the steady state fraction of attached motors is $\rho_a/\rho_m = \omega^0_{\text{on}}(\omega^0{}_{\text{on}} + \omega_{\text{off}})^{-1}$. In the absence of any mean motor deformation (ie., when $Y_0 = 0$ so that $\mathcal{F} = 1$), this fraction equals $\omega^0_{\text{on}}(\omega^0{}_{\text{on}} + \omega^0_{\text{off}})^{-1}$ providing the mapping between the frequency of attachment/detachment in the continuum theory and probabilities of attachment and detachment in the stochastic simulation. However, we note that despite being a discretized model, the segments in the filament still represent a coarse grained description of the filament in biological systems and hence we allow multiple motor heads to occupy the same site on the filament. Because of the initial distribution of the motors, the torque on the filament due to motor activity is negligible and the system is essentially one dimensional.

For simplicity and to focus on the role of activity and noise, we did not incorporate permanent passive cross-linkers of the

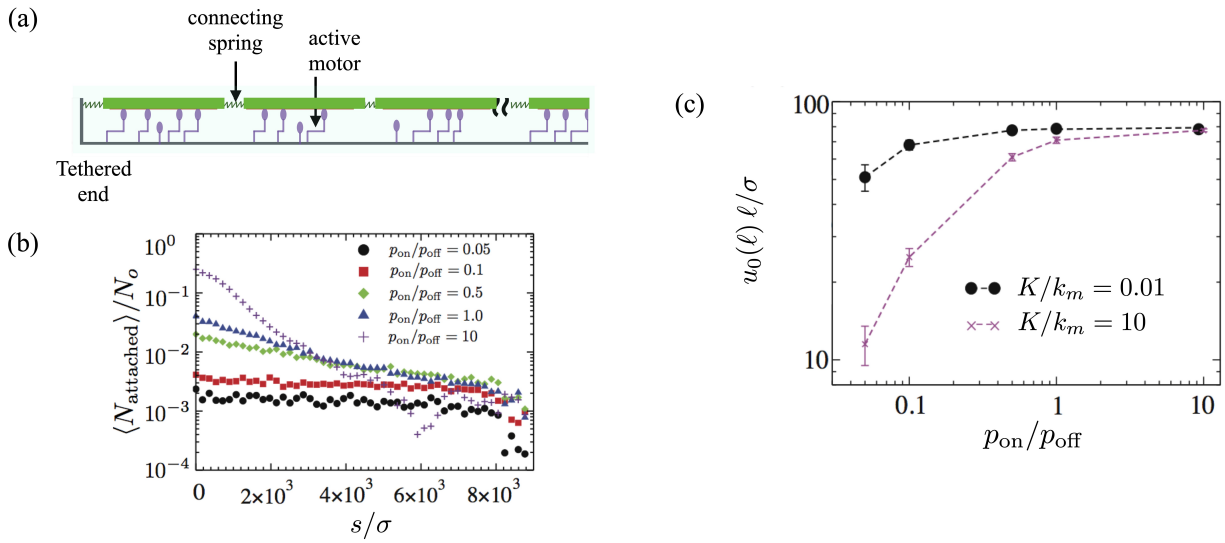

Figure 5: (a) Sketch of a discrete, active composite filament we analyze in this paper. The composite filament is made of 50 similar rigid segments each connected to its neighbors by a linear elastic spring with spring constant K. One end of the segment (Index 1) is anchored to a wall by a similar spring while the other (free) end (Index 50) is oscillated with a frequency ω. Each segment interacts with 80 active motors that periodically attach and detach from the filament. (b) The fraction of motors attached on the composite filament $\langle N_a \rangle$, as a function of their position from the clamped end for $K/k_m = 10$. The mean motor attachment is maximum close to the clamped end, where the local strain is relatively small. (c) Time averaged steady state extension of the segment at the free end, $\langle u_0(\ell) \rangle$, as a function of zero load motor attachment/detachment probability, $p_{\text{on}}/p_{\text{off}}$, for various values of passive spring stiffness, K/k_m. The extension increases with $p_{\text{on}}/p_{\text{off}}$, and decreases with K/k_m, consistent with analytical predictions. For large $p_{\text{on}}/p_{\text{off}}$ the extension saturates at a maximum value, set by the finite length of the filament-motor composite.

mean-field model. This the simulation corresponds to the limiting case $\rho_N = 0$. This does not change the qualitative features of the solution since, shear resistance is always provided by active motors when attached. With this simplification, the passive elasticity of the filament is contributed solely by the weak extensional elasticity of the filament. We point out that the simulation is truly one dimensional since we simulate a bead-spring filament of thickness a rather than a quasi-1D strip of width $b \gg w$ considered in the theory.

The time dependent evolution of this system of motors and segments are analyzed in the over-damped limit using Brownian Multi-particle Collision Dynamics (Brownian-MPC) method (43). This method neglects long range hydrodynamic interactions between the segments while keeping the system in a thermal bath. According to this scheme, each monomer beads of the segment independently performs a stochastic collision with phantom fluid particles with momenta taken from the Maxwell-Boltzmann distribution with variance $\rho k_b T$, ρ being the phantom fluid density. In between these collision events, the monomer positions velocities are updated using standard molecular dynamics (MD) scheme. The timescale for Brownian-MPC simulation $t_{\text{MPC}} = \sqrt{m\sigma^2/k_B T}$, where m is the mass of a phantom-fluid particle, a is the diameter of the monomer bead which equals the length-scale arises from the discretization of space in the simulation scheme (43). However, the physical timescale relevant to this problem is the numerically calculated thermal relaxation time of the segment of length $80\,a$, which is much larger than t_{MPC}. This relaxation time is determined by the viscosity of the medium set by the simulation parameters (43, 44). For the same set of fluid parameters used in reference (44), we find the relaxation time, τ, of the segment of length 80σ to be about $4.6 \times 10^3 t_{\text{MPC}}$.

4.2 Identifying a suitable stationary stable deformed state

As in our mean field theory §3.5.1 and §3.5.2, we first study the dynamics of a single, rigid segment of length $\ell_s = 80\,\sigma$, driven by an aggregate (75-800 in number thus corresponding to different motor densities) of active motors. The segment is animated by an array of motors, and moves against a resisting linear elastic spring with spring constant K_s. One end of the segment is attached to this spring (see ESM Figure 1(b)) while the other end is free. The spring meanwhile is anchored to a wall and has a zero rest length. In this stochastic model, the passive shear springs are not incorporated.

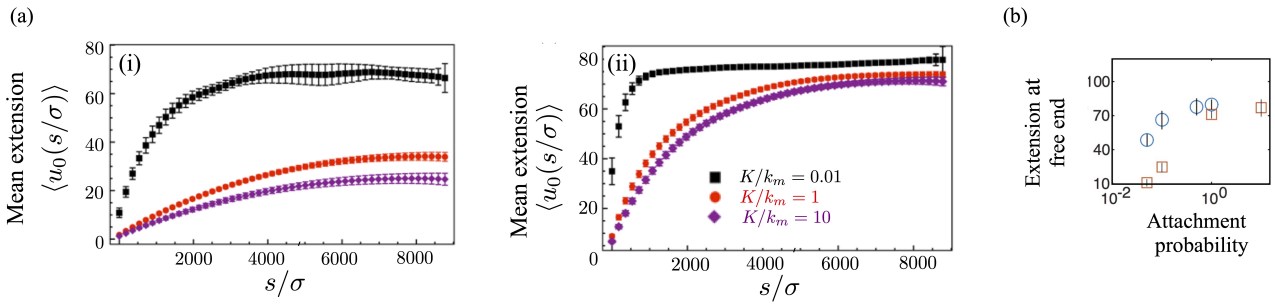

Figure 6: (a) The dimensionless mean steady state extension of material points $\langle u_0(s)\rangle \ell/a$ as a function of their position from the clamped end $s = 0$ for three values of $p_{\rm on}/p_{\rm off}$ - (i) 0.1 and (ii) 1.0. Vertical bars correspond to the root mean square deviation and indicate the extent noise plays in disturbing the mean value. Other parameters correspond to Figure 5. (b) The extension at the free end as a function of attachment probability $p_{\rm on}$ for soft ($K/k_m = 0.01$, circles, online-blue) and stiff ($K/k_m = 10$, squares, online-red) filaments.

Motor activity results in the sliding motion of this rigid segment. This motion is coupled to the deformation of the anchoring spring. The dynamical response of this system is studied as a function of two parameters, a stiffness parameter K_s/k_m and the activity parameter $p_{\rm off}/p_{\rm on}$. This is done by tracking the displacement of the segment as a function of time as well as the temporal variations in the fraction of active motors attached to the segment. Times are scaled using $\tau \simeq 4.6 \times 10^3 t_{\rm MPC}$. This simulation allows us to characterize the dynamical regimes of that segment as a function of motor activity and elastic stiffness. More importantly, this allows us to identify the appropriate base state to use in our calculation of the decay lengths of imposed or inherent local extensional strains.

Depending on the values of K_s/k_m and $p_{\rm off}/p_{\rm on}$ we find three distinct dynamical regimes as illustrated in Fig. 4(a). For a fixed value of K_s/k_m when $p_{\rm off}/p_{\rm on} \ll 1$ a majority of the motors are attached to the filament, subjecting the segment to a significant active force. Consequently, the segment displays a steady extension. In the complementary limit, where $p_{\rm off}/p_{\rm on} \gg 1$ the re-attachment rate of the motors is small, causing a majority of the motors to be in the detached state. Thus, in the absence of any significant extensional force the filament attains a steady, but non-extended state. However there is a third time dependent regime observed for intermediate values of $p_{\rm off}/p_{\rm on}$; in this regime, we observe intermittent (Fig. 4(a)-middle) or regular (Fig. 4(a)-top) oscillations of the segment with concomitant extension and compression of the linear spring. These oscillations are quantified by measuring the distance of the free end of the filament from the anchor point (Δ_a) as a function of time. The stable, regular oscillatory state is marked by a well defined frequency while in the intermittent oscillatory state, the segment randomly switches between stationary and oscillatory states.

Figure 4(b) explores the complementary phase space where the number of motors is kept fixed (at 800) while the ratio K_s/k_m is varied. We observe that oscillations for fixed motor density can be triggered or suppressed by tuning the ratio K_s/k_m. The striking difference between the theoretical predictions and the simulation results is the presence of an intermittently oscillating state (yellow, diamonds). A sweep of the parameter space yields the computational phase plot in Figure 4(c) that maps the regimes in the space spanned by the ratio $p_{\rm off}/p_{\rm on}$ and the number of motors. This plot is qualitatively consistent with the theoretically predicted plot shown in Figure 3(a) and Figure 3(b)-(i). Recognizing the equivalence of Ψ and the ratio $p_{\rm off}/p_{\rm on}$, we note that for a fixed number of *total* motors equivalent to a fixed stiffness parameter oscillations (red, squares) are observed only for a range of Ψ. In the absence of noise, the boundary in parameter space between stationary and oscillatory states is sharp. Discrete noise however smears this sharp boundary and renders it fuzzy. Thus the intermittent states are sustained by noise - here due to the discrete motor binding and unbinding events and due to the finite number of motors. We emphasize that there is no thermal noise in the system and anticipate that the presence of thermal noise will probably broaden the intermittent region further. Focusing on the regular oscillatory regime, we also compute the frequency as a function of the $p_{\rm off}/p_{\rm on}$ at fixed stiffness ratio as shown in Fig. 4(d) and find that the response is consistent with the mean-field predictions, with frequency of oscillations ω_a increasing with the ratio $p_{\rm off}/p_{\rm on}$. This may be compared to Figure 3(b)-(ii) where we found that oscillation frequency was predicted to increase almost linearly with increasing values of Ψ.

The physical picture underlying the onset of these oscillations may be understood as follows. The motion of the filament due to motor activity results in a non-linear viscoelastic coupling between the motors, the spring and the irreversible motor friction. At criticality, the motion is determined by the linear response to small perturbations. In this limit, the viscoelastic coupling may be reduced to effective, linear, in-phase (effective elastic) as well as out of phase (viscous) compliance terms. Oscillations arise

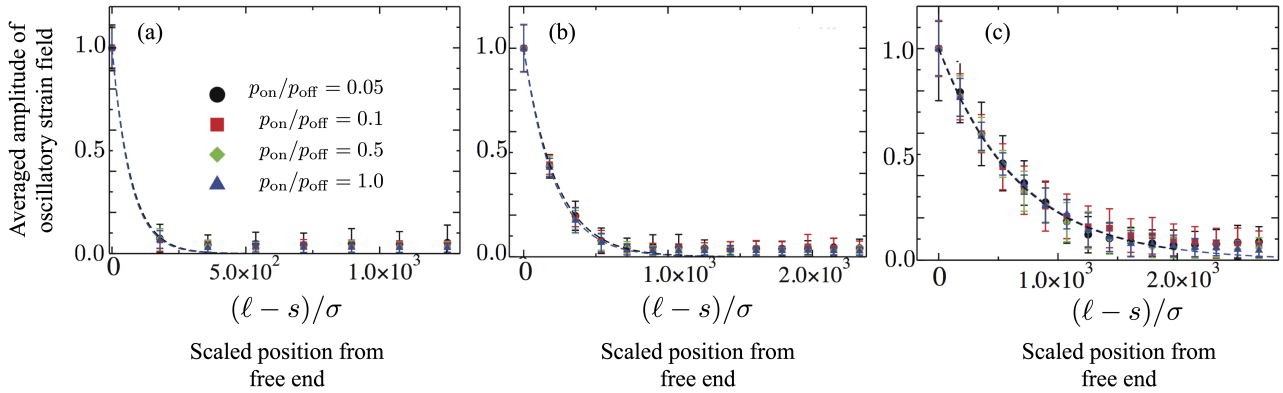

Figure 7: (a)-(c) The noise averaged amplitude of spatial oscillatory field of the filaments as a function of position s, for different values of the stiffness parameter - i.e., the elasticity contrast (a) $K/k_m = 10^{-3}$, (b) 10^{-2} and (c) 10^{-1}. Here ℓ is the total length of the composite filament - we note this allows us to define an average coarse-grained elastic modulus per length. The dashed curves show exponential fits indicating decay lengths whose value depends on motor kinetics via the ratio of attachment to detachment probabilities as well as on the elasticity contrast. The (dimensionless) forcing frequency is $10^{-3}\ v_0/\sigma$.

when either of these terms turn negative as a result of positive feedback. When the system is in the stable oscillatory state, the power input to the system due to motor activity balances the energy dissipated due to frictional damping caused by motor attachment. Invoking expressions from the continuum theory presented earlier, we estimate the active friction due to motors to be $\eta_{\text{act}} \sim \rho_m N_0 k_m (d\langle y\rangle/du_t)_{u_t=0}$ where $u_t = du/dt$ and $\rho_m N_0$ is the total number of attached motors. As Ψ increases, both N_0 and $(d\langle y\rangle/du_t)_{u_t=0}$ are expected to typically decrease, and therefore the frequency of the emergent oscillations should increase.

4.3 Persistence of steady deformations in noisy active filament-motor composites

Having identified the dynamical regimes of a single rigid segment, we now analyze the dynamical behavior of a long, extensible composite filament as sketched in Fig. 5(a). This composite filament is made up of 50 rigid segments, each of length 80σ. The anchored end is chosen to correspond to $s = 0$ while the free end corresponds to $s = \ell$. The variable s here thus measures distance from the anchored end and is identical to the arc-length parameter introduced in the continuum model.

As before, the overall global softness of the filament is controlled by the elastic constant of connecting springs, here denoted by K and proportional to the modulus K_{pas} in the continuum mean-field theory. We distribute 80 motors uniformly on each of the segments and choose simulation parameters such that the dynamical state of each of the segments corresponds to steady, non-oscillatory extension, $u_0(s)$. The choice of the parameters is guided by the results for the unit cell (single segment) case. The base state chosen was confirmed to be stationary so that each segment as well the the whole composite filament is free of oscillatory instabilities. Due to the stochastic nature of the motor dynamics, all the steady quantities have a fluctuating component. We measure the mean of these quantities by taking a time average after the system has evolved into a steady state.

Since the motor kinetics is coupled to the inhomogeneous filament strain, the motor imposed filament extensions modifies the number of attached motors on the filament. In Fig. 5(b) we plot the mean fraction of motors attached, $\langle N_a\rangle$, as a function of t s for $K/k_m = 10$ and for different values of $p_{\text{on}}/p_{\text{off}}$. When $p_{\text{on}}/p_{\text{off}} < 0.1$ the motor imposed extension of the filament is weak as the number of attached motors is small and the motor distribution is roughly uniform along the filament. However when $p_{\text{on}}/p_{\text{off}} > 1$ the enhanced motor attachment imposes significant extension to the filament, which is maximum at the free end. The nonuniform extension of the composite leads to a nonuniform distribution of attached motors with the mean motor attachment is maximum near the anchored end ($s = 0$), where the filament extension is minimum as seen in Fig. 5(c). The attached fraction decreases with the distance from that point as the filament strain increases as one moves towards the free end.

The time averaged steady motor induced extension $\langle u_0(s)\rangle$ of the filament as a function of the stiffness parameter K/k_m are plotted in Fig. 6(a)-(i) & (ii) for two values of $p_{\text{on}}/p_{\text{off}}$. Note that p_{off} is constant in these plots; the ratio is changed by varying just the detachment probability. As seen already in Fig. 5(c), filament extension is minimum near the clamped end and maximum at the free end; furthermore both $p_{\text{on}}/p_{\text{off}}$ as well as K/k_m equally influence the value as well as the gradient in the extensional strain. In general, u_0 increases with the fraction of attached motors ($\propto (p_{\text{off}}/p_{\text{on}})^{-1}$) and filament softness $\propto (K/k_m)^{-1}$. In continuum limit, as anticipated by the mean-field theory (see ESM §3) the steady state extension (u_0) in the

limit of no permanent cross-linkers is

$$u_0(s) \propto \left(\frac{\rho_m k_m}{2K}\right) s(2\ell - s) \tag{36}$$

where the constant of proportionality depends purely on motor kinetics and is independent of position. Note that this form is also evident from equation (34) where motor activity and kinetics appears as a pre-factor multiplying the function that encodes the spatial variation. In our simulation, we do not have passive linkers and this $\rho_N = 0$. Therefore, $u_0(s)$ does not have any have a characteristic decay length; this is because attached active motors form only temporary attachments and do not contribute to the long time filament (shear) elasticity. The discrete nature of motor activity causes large fluctuations in mean extension of the filament, especially for very soft filaments with $K/k_m \ll 1$. We also find from additional simulations that motor noise results in uncorrelated spatial domains for $K/k_m = 0.01$ while a greater degree of correlation is observed for $K/k_m = 10$.

The Brownian-MPC simulations are an improvement over the mean-field theory in an important way; in the theory, the local attachment fraction was spatially invariant and independent of position along the filament. In our case, the coupling between elasticity and motor kinetics is intrinsic and non-linear. A consequence of this is the strong variation of the attached motor fraction with position from the clamped end evident in Figure 6(b) for high attachment probabilities. Note also that the quadratic nature of extension field, predicted from mean-field theory is qualitatively consistent with the numerical results. Allowing for the attached motor fraction to vary with position allows one to incorporate some non-linear coupling effects and predict the deviation from the quadratic scaling of the extensional strains closed to the clamped end.

4.4 Decay lengths of oscillatory strains

To study the decay of localized oscillatory strains in this noisy, active setting we simulate the model problem analyzed in § 3.5.3. We impose a low frequency ($\omega \ll v_0/\sigma$), small amplitude ($u_1 \ll u_0(\ell)$) oscillation at the free end ($s = \ell$) about the steady stationary extension that is attained in the absence of this imposed deformation. Thus, the net extension imposed (and measured) at the free end is $u(\ell) = u_0(\ell) + u_1 \sin(\omega t)$. Since the motors do not form permanent cross-links, this steady state deformation is identical to the deformation attained as the frequency goes to zero. The oscillation at $s = \ell$ results in a spatially and temporally varying extensional field $u(s)$ along the contour of the filament. At long times, after initial transients have died out, this field may be written as the sum of the actively generated steady strain u_0 and an oscillatory strain of amplitude $\hat{u}(s) \propto u_1$. For small deformations, the ratio $\hat{u}(s)/u_1$ depends only on s, the filament elasticity and motor kinetics. In the frequency-locked limit $\hat{u}(s)/u_1$ oscillates with frequency ω - the critical assumption here is that intrinsic oscillatory instabilities are not excited due to motor activity.

Focusing on the amplitude $\hat{u}$ of the oscillatory part of the strain, we compute the spatial variation and fluctuations (averaged over many motor cycles) in the amplitude for each segment as a function of its distance from the free end ($\ell - s$). For sufficiently low frequencies, the results are qualitatively independent of the frequency ω as the system is truly frequency-locked. For high frequencies, we observed that in some cases localized oscillations were initiated - for these systems the notion of a persistence length breaks down and is not a useful physical measure. Hence we will focus on the low-frequency results and in particular the value $\omega = 10^{-3}(\sigma/v_0)$. In the case of an inextensible filament, the oscillatory strain that is imposed at the free end would propagate an infinitely long distance without any decay in its amplitude. However, for finitely extensible filaments, equation (29) predicts an exponential decay of strain along the filament. Indeed, simulations confirm this feature. Figures 7(a)-(c) show an exponential decay for the scaled amplitude of the oscillatory extension $\hat{u}/u_1$ as a function of distance from the free end for different values of K/k_m and $p_{\text{on}}/p_{\text{off}}$. The amplitude $\hat{u}$ does show large fluctuations due to the noise imposed by discrete motor attachment/detachment - something the mean-field theory cannot capture.

The length scale over which the elongation decays λ_E is seen to be a strong function of K/k_m, but surprisingly, only a weak function of $p_{\text{on}}/p_{\text{off}}$ in the regime we probed. We hypothesize that this is because the system has access to the dynamical parameter space where the average number of attached motors is small and the contribution to the elastic stiffness due to motor attachment is negligible.

4.5 Coherence and decay lengths

The decay of steady, motor-mediated, localized extensions is controlled by K/k_m and the ratio of detachment to attachment probabilities, $p_{\text{off}}/p_{\text{on}}$, for both stiff ($K/k_m = 10$) and soft ($K/k_m = 10^{-2}$) filaments. The mean field prediction is qualitatively consistent with the simulation results for $p_{\text{off}}/p_{\text{on}} \sim 1$ with deviations seen for large contrasts between the probabilities. Increasing the attachment probability results in a larger fraction of attached motors with sharper gradients near the clamped end and flatter profiles near the free end consistent with analytical predictions. Motor noise results in large fluctuations in the mean extension, noticeable especially for the soft filaments and also results in uncorrelated spatial domains in extension as demonstrated in Figures 8(a) and 8(b).

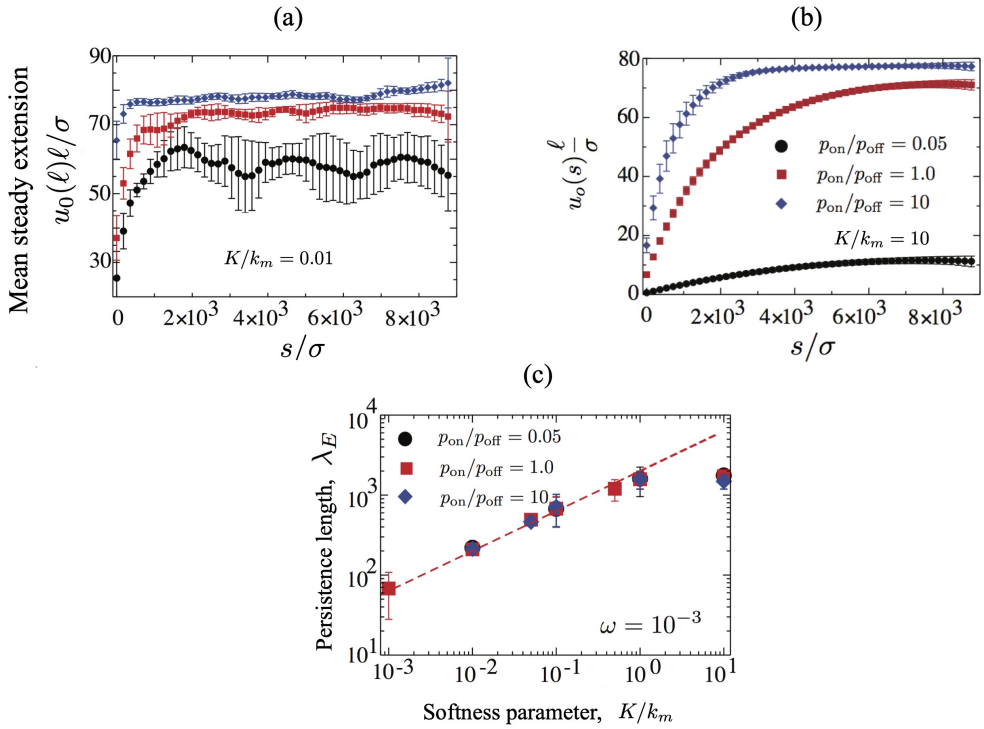

Figure 8: Summary of our results (a,b) Scaled mean steady extension as a function of position from the clamped end. Vertical bars correspond to the RMS deviation. Extensions are observed to be uncorrelated for soft assemblies ($K/k_m = 0.01$) with domains fluctuating independently. Increasing stiffness allows separated parts of the filament to move more in consort. Note that changing the motor kinetics also affects the size of these independent domains. The strain gradient localizes close to the clamped end for soft assemblies, especially for large attachment probabilities. We expect large fluctuations (induced or arising intrinsically) to have more of an effect in disrupting coherent behavior in these domains. (c) Decay lengths λ_E obtained by analyzing the amplitude of oscillations as a function of K/k_m for various p_{on}/p_{off}. For small values of the ratio (weak elasticity) the simulations agree with the theoretical scaling predictions, $\lambda_E \propto \sqrt{2K/k_m\rho_m}$ shown as the dashed line. We see evidence of system size saturation for large values of K/k_m and hence the deviation from the mean-field prediction. The (dimensionless) forcing frequency of the oscillation at the end is $10^{-3}v_0/\sigma$. Results are qualitatively similar for small forcing frequencies. As the frequency increases, the frequency-locked response may not be a valid assumption and the concept of a decay length loses its significance.

For small (fixed) ω, we estimate the decay length λ_E by fitting $\hat{u}(\ell - s)$ to an exponentially decaying function, and extract decay lengths for a range of K/k_m and p_{on}/p_{off}. Our calculations show an increase in λ_E as K/k_m is varied from 10^{-3} to 10. We plot the computationally calculated λ_E for this moderately noisy system as a function of K/k_m in Fig. 8(c). The analytical prediction (32) for $G_{pas} = 0$ may be written in the form

$$\lambda_E \propto \sqrt{2\frac{K}{k_m\rho_m}}. \tag{37}$$

Our simulation results shows excellent agreement with this prediction for almost all of the range explored in K/k_m. For very stiff filaments, we find that the computational value deviates from the dashed line and seems to saturate to a constant. We ascribe this behavior to finite system size effects. The constant of proportionality in (37) is dependent purely on motor properties and the excitation frequency. To confirm this, we also computed the decay length for imposed frequencies (dimensionless) $\omega = 10^{-2}$ and found qualitatively similar results. For instance, when $K/k_m = 1$, the decay length is proportionally smaller than for $\omega = 10^{-3}$ due to the dependence of χ on the frequency.

5 CONCLUSION

The scale over which local active deformations persist in a fluctuating elastic network is a fundamental question that arises in the study of living, active and activated matter. Here, this question is addressed in the context of an ordered composite structure consisting of elastic elements that can be stretched and sheared by active motors binding to and unbinding from them. We present a mean-free theory in the weak noise and weakly elastic limit as well as detailed Brownian multi-particle collision dynamics-based numerical simulations for noisy, moderately soft and soft composites. Both theory as well as simulations show that extensibility may be negligible locally but it cannot be ignored globally. In nearly stiff filaments for which extensional stains are negligible, the interplay between activity and shear elasticity can result in stable stationary or oscillatory extensions. Motor noise due to discrete binding and unbinding events and due to finite motor numbers results in a fuzzy boundary exhibiting intermittency between these two stable regimes. This suggests that localized, bounded oscillations may arise naturally in long filaments. The decay of such naturally emergent or imposed oscillatory as well as steady extensions in long filaments is determined by passive as well as active elastic components.

In the absence of permanent cross-links, we find no decay length for steady extensions even when active motors form temporary cross links. When permanent elastic links are present, the decay length depends on the extensional modulus of the filament and the shear modulus due to the permanent cross-links. Consistent with theoretical predictions, our simulations show that the ability of attached motors to sense local extension rates influences the motor activity and modifies the effective length scale over which strain decays. While the numerical model shows deviations from noiseless mean field predictions due to the presence of strong discrete noise caused by the variations in individual motor activity, several qualitative features are surprisingly still retained. Specifically, for fixed motor attachment and detachment rates, the decay length is set by the ratio of the passive elastic modulus of the constituent filament to the active shear modulus generated by attached motors - even in the presence of noise. This confirms a finite range for correlated activity that might be relevant for natural examples of ordered active matter such as eukaryotic flagella (4) by setting a limit over which mechanical coordination can persist. It also raises interesting questions about how to generalize our analysis to the deformations of bio-filaments in living matter such as bacterial swarms (45) and disordered mixtures of motors and cytoskeletal filaments (46, 47), particularly in the limit when the coordination number is small and when it approaches the isostatic limit. Our results also are relevant to understanding the general mechanisms by which motor activity may stiffen or soften fiber networks (48, 49), in studies on persistence lengths in active filamentous systems (50–52), and in understanding how the decay of substrate strain induced due to contractility may coordinate the motions of cells (54, 55).

AUTHOR CONTRIBUTIONS

AG, RC and LM designed the research and formulated the research questions. AG formulated the mean field theories for active and passive composites. RC formulated the stochastic MPC model and carried out all simulations. AG, RC and LM analyzed the data and wrote the paper.

ACKNOWLEDGMENTS

AG would like to acknowledge partial support from NSF via grant NSF-MCB-2026782.

REFERENCES

1. J. Howard, *Mechanics of motor proteins and the cytoskeleton*, (Sinauer Associates), ISBN 0878933344.

2. G. B. Witman, *Introduction to cilia and flagella in ciliary and flagellar membranes* (ed. R. A. Bloodgood), Plenum, New York, pp 1-30 (1990).

3. J. Howard (2008) Molecular mechanics of cells and tissues. Cell. Mol. Bioeng., 1(1): 24-32.

4. D. M. Woolley (2007) A novel motility pattern in quail spermatozoa with implications for the mechanism of flagellar beating. Biol. Cell, 99(12), 663-675.

5. R. Everaers, R. Bundschuh and K. Kremer (1995) Fluctuations and stiffness of double-stranded polymers: railway-track model. Europhys. Lett., 29 (3): 263-268.

6. L. Scharrel, R. Ma, R. Schneider, F. Jülicher and S. Diez (2014) Multimotor Transport in a System of Active and Inactive Kinesin-1 Motors. Biophys. J., 107:365-372.

7. C. Heussinger, M. Bathe and E. Frey (2007) Statistical mechanics of semiflexible bundles of wormlike chains. Phys. Rev. Lett., 99(4): 048101.

8. H. Mohrbach and I. M. Kulic (2007) Motor driven microtubule shape fluctuations: force from within the lattice. Phys. Rev. Lett., 99(21): 218102.

9. A.Vilfan and E. Frey (2005) Oscillations in molecular motor assemblies. J. Phys. Condens. Matter, 17(47):S3901-S3911.

10. S. W. Grill, K. Kruse and F. Jülicher (2005) Theory of mitotic spindle oscillations. Phys. Rev. Lett., 94(10): 108104.

11. E. Evans, K. Ritchie (1997) Dynamic strength of molecular adhesion bonds. Biophys. J., 72(4):1541-1555.

12. F. Gittes, B. Mickey, J. Nettleton and J. Howard (1993) Flexural rigidity of microtubules and actin filaments measured from thermal fluctuations in shape. J. Cell Biol., 120(4): 923-934.

13. C. J. Brokaw (1975) Molecular mechanism for oscillation in flagella and muscle. Proc. Natl. Acad. Sci. USA, 72(8): 3102-3106.

14. C. J. Brokaw (1989) Direct measurements of sliding between outer doublet microtubules in swimming sperm flagella. Science, 243(4898):1593-1596 .

15. C. J. Brokaw (1971) Bend propagation by a sliding filament model for flagella. J. Exp. Biol., 55:289-304.

16. H. Kojima, M. Kikumoto, H. Sakakibara, K. and Oiwab (2002) Mechanical properties of a single-headed processive motor, inner-arm dynein subspecies-c of chlamydomonas studied at the single molecule level. J. Biolog. Phys., 28(3): 335-345.

17. H. Sui and K.H. Downing (2006) Molecular architecture of axonemal microtubule doublets revealed by cryo-electron tomography. Nature, 442(7101): 475-478.

18. K.E. Machin (1963) The control and synchronization of flagellar movement. Proc. Roy. Soc. B., 158(970), 88-104.

19. V. Mukundan, P. Sartori, V. F. Geyer, F. Jülicher, and J. Howard (2014) Motor regulation results in distal forces that bend partially disintegrated chlamydomonas axonemes into circular arcs. Biophys. J., 106:1-9.

20. B. Qin, A. Gopinath, J. Yang, J. P. Gollub, and P. E. Arratia (2015) Flagellar kinematics and swimming of algal cells in viscoelastic fluids. Scientific Reports 5.

21. H. Yoke and C. Shingyogi (2017) Effects of external stress on the regulation of microtubule sliding induced by outer arm dynein of sea urchin sperm flagella. J. Exp. Biol., 220(6): 1122-1134.

22. M. J. Wargo, M. A. McPeek and E. F. Smith (2004) Analysis of microtubule sliding patterns in Chlamydomonas flagellar axonemes reveal dynein activity on specific doublet microtubules. J Cell Sci., 117: 2533-2544.

23. P. Satori, N. F. Geyer, A. Scholich, F. Julicher and J. Howard (2016) Dynamic curvature regulation accounts for the symmetric and asymmetric beats of Chlamydomonas flagella. eLife 5: e13258.

24. D. M. Woolley (2010) Flagellar oscillation: a commentary on proposed mechanisms. Biol. Rev. Camb. Philos. Soc.. 85: 453-470.

25. P. Satir, T. Heuser, W. S. Sale (2014) A structural basis for how motile cilia beat. BioScience, 64: 1073- 1083.

26. S. M. King (2018) Turning dyneins off bends cilia. Cytoskeleton, 75: 372-381.

27. Y. Man, F. Ling and E. Kanso (2019) Cilia oscillations. Phil. Trans. Roy. Soc. B, 375: 20190157.

28. J. Lin, K. Okada, M. Raytchev, M. C. Smith and D. Nicastro (2014) Structural mechanism of the dynein power stroke. Nat. Cell Biol., 16: 479.

29. J. Lin J and D. Nicastro (2018) Asymmetric distribution and spatial switching of dynein activity generates ciliary motility. Science, 360 (6387): eaar1968.

30. K. W. Foster, J. Vidyadharan and A. Sangani (2017) Evidence for a self-organized compliant mechanism for the spontaneous steady beating of cilia. Cell Motil. and Cytoskel., 74(7): 260-280.

31. R. Coy and H. Gadêlha (2017) The counterbend dynamics of cross-linked filament bundles and flagella. J. R. Soc. Interface, 14: 20170065.

32. M. Bottier, K. A. Thomas, S. K. Dutcher and P. V. Bayly (2019) How does cilium length affect beating? Biophys. J., 116: 1292–1304.

33. P. V. Bayly and K.S. Wilson (2014) Equations of interdoublet separation during flagella motion reveal mechanisms of wave propagation and instability. Biophysical J. 107, 1756.

34. P. V. Bayly and S. K. Dutcher (2016) Steady dynein forces induce flutter instability and propagating waves in mathematical models of flagella. J. Royal Soc. Interface 13, 20160523.

35. M. Bathe, C. Heussinger, M. M. Claessens, A. R. Bausch and E. Frey (2008) Cytoskeletal bundle mechanics. Biophys. J., 94(8): 2955.

36. C. Heussinger, F. Schüller and E. Frey (2010) Statics and dynamics of wormlike bundle model. Phys. Rev. E., 81(2): 021904.

37. A. Ward, F. Hilitski, W. Schwenger, D. Welch, A. W. C. Lau, V. Vitelli, L. Mahadevan and Z. Dogic (2015) Solid friction between soft filaments. Nat. Mater., 14, 583-588.

38. E. Reissner (1946) Analysis of shear lag in box beams by the principle of minimum potential energy. Quart. J. of Applied Math., 4:268-278.

39. K. Hatch, C. Danilowicz, V. Colijee and M. Prentiss (2008) Demonstration that the shear force required to separate short double-stranded DNA does not increase significantly with sequence length for sequences longer than 25 base pairs. Phys. Rev. E, 78(1):011920.

40. C. B. Lindemann, L. J. Macauley and K. A. Lesich, (2005) The counterbend phenomenon in dynein-disabled rat sperm flagella and what it reveals about the interdoublet elasticity. Biophys. J., 89(2):1165-1174.

41. S. Camalet and F. Jülicher (2000) Generic aspects of axonemal beating. New J. Phys., 2: 24.1-24.23.

42. I. H. Riedel-Kruse, A. Hilfinger, J. Howard and F. Julicher (2007) How molecular motors shape the flagellar beat. HFSP Journal, 1(3):192-208.

43. G. Gompper, T. Ihle, D. M. Kroll and R. G. Winkler (2008) Multi-particle collision dynamics: a particle-based mesoscale simulation approach to the hydrodynamics of complex fluids. Adv. Polym. Sci., 221:1-87.

44. R. Chelakkot, R. G. Winkler and G. Gompper (2010) Migration of semiflexible polymers in microcapillary flow. Eur.Phys.Lett., 91: 14001.

45. A. E. Patteson, A. Gopinath and P. E. Arratia (2018). The propagation of active-passive interfaces in bacterial swarms Nature Communications, 9 (1), 5373.

46. T. Sanchez, D. Welch, D. Nicastro and Z. Dogic (2001) Cilia-like beating of active microtubule bundles. Science, 333(6041): 456-459.

47. T. Sanchez, D. T. N. Chen, S. J. DeCamp, M. Heymann and Z. Dogic (2012) Spontaneous motion in hierarchically assembled active matter. Nature, 491(7424): 431-434.

48. C. P. Broedersz and F. C. Mackintosh (2011) Molecular motors stiffen non-affine semiflexible polymer networks. Soft Matter, 7:3186.

49. C. A. Weber, R. Suzuki, V. Schaller, I. S. Aranson, A. R. Bausch and E. Frey (2015) Random bursts determine dynamics of active filaments. PNAS 112(34):10703-10707.

50. C. Li, B. Qin, A. Gopinath, P. E. Arratia, B. Thomases and R. D. Guy (2017) Flagellar swimming in viscoelastic fluids: role of fluid stress revealed by simulations based on experimental data. Proc. Roy. Soc. Interface., 14(135): 20170289.

51. S. Fatehiboroujeni, A. Gopinath and S. Goyal (2021) Three-dimensional nonlinear dynamics of prestressed active filaments: flapping, swirling, and flipping. Physical Review E 103 (1), 013005.

52. X. Liao, P.K. Purohit and A. Gopinath (2020) Extensions of the worm-like-chain model to tethered active filaments under tension. Journal of Chemical Physics 153, 194901

53. C. Bouchiat, M. D. Wang, A.-F. Allemand, T. Strick, S. M. Block and V. Croquette (1999) Estimating the Persistence Length of a Worm-Like Chain Molecule from Force-Extension Measurements. Biophysical J., 76:409-413.

54. S. Bose, K. Dasbiswas and A. Gopinath (2021) Matrix Stiffness Modulates Mechanical Interactions and Promotes Contact between Motile Cells. Biomedicines 9:428.

55. S. Goren, Y. Koren, X. Xu and A. Lesman (2020) Elastic anisotropy governs the range of cell-induced displacements. Biophysical Journal 118: 1152–1164.

SUPPLEMENTARY MATERIAL

An online supplement to this article can be found by visiting BJ Online at http://www.biophysj.org.